Recovering of weather degraded images based on RGB response ratio constancy

Raúl Luzón-González,* Juan L. Nieves, and Javier Romero

University of Granada, Department of Optics, Granada 18072, Spain

*Corresponding author: raul@ugr.es

Images captured under bad weather conditions suffer from poor contrast and visibility. These effects are noticeable for haze, mist, fog, or dust storms. We have proposed a recovering method for images captured for several adverse weather conditions based on the RGB response ratio constancy under illuminant changes. This algorithm improves the visibility, contrast, and color in degraded images with low computational times. We obtain results similar to those from previously published deweathering methods but with no prior information about the image content or atmospheric parameters needed.   © 2015 Optical Society of America

OCIS codes: (100.2000) Digital image processing; (100.2960) Image analysis; (100.2980) Image enhancement.
http://dx.doi.org/10.1364/AO.54.00B222

1. Introduction

Nowadays digital cameras are used in a plethora of systems, such as surveillance systems, user aid systems, and customer devices, just to mention some applications. Digital images add many advantages in the way we manage the information contained in the scenes, allowing us to obtain object structure information or material recognition. In some circumstances the outdoor images could be affected by bad weather conditions and the objects in the scene far away from the observer could decrease their visibility. Under these situations, captured images could have not enough quality to be useful, having poor contrast or dimmed colors. Reduction of the objects' contrast and the alteration of the objects' color is a consequence of the interaction between the light and the particles present in the atmosphere. As is easily noticeable, when the objects are far away from the observer their chromaticity turns into the chromaticity of the horizon, exhibiting the typical shift to bluish or whitish in the objects' hue [1]. This is an old topic used in arts to obtain the depth sensation [2]

and is widely studied in atmospheric optics [3,4]. Under adverse conditions, intuitively we can suppose that the light coming from the objects suffers more interactions (dense atmospheric paths) with the atmospheric particles, so less information coming from the objects impinges directly on the observer. For extreme situations, such as very thick fog, the objects could hardly be visible or even become invisible. As a consequence, weather recovering algorithms (sometimes called deweathering algorithms in the literature [5]) should be used as a previous step in such systems to get reliable information under weather affected images.

In the field of weather restoring images there are two main approximations: one based on nonphysical models and another one based on physical models. Histogram equalization and its variations [6,7] are the most widespread nonphysical models. Recently, several works were based on retinex theory to improve brightness [8,9], contrast, and sharpness of weather degraded images. The main drawback of these algorithms lies in the restoration of the original objects' color in the scene, particularly when the objects are situated at different planes. Improved results have been obtained employing physical-based models [10]. The most successful methods rest on

the dichromatic atmospheric scattering model [11]. This model postulates that the light impinging in the observer coming from an object is composed of two terms: one direct term coming from the object but attenuated by the atmosphere, plus another term that adds light in the cone of vision of the observer. The first term, usually denoted as attenuation, is more noticeable at short distances. As objects become farther away from the observer, their color information gets lost, and their chromaticity tends to the chromaticity of the horizon. The second term, usually denoted as the airlight term, is more important at long distances and has no spectral information of the objects.

In the image restoring field, the dichromatic atmospheric scattering model is usually depicted as [12,13]

$$I^c(x, \lambda) = J^c(x, \lambda)t(x, \lambda) + A^c(1 - t(x, \lambda)), \qquad (1)$$

where x denotes the 2D pixel coordinates in the image, λ is the wavelength of the incident light, c stands for the camera channel (c will be just one channel for gray-scale images, or $c = $ R, G, or B for full color images), I is the captured image, J is the radiance coming from the object, t is the transmittance factor, and A is the horizon radiance. The transmittance of the medium is expressed as

$$t(x, \lambda) = \exp(-\beta(\lambda)d), \qquad (2)$$

where β is the extinction coefficient, related to the size and density of the particles present in the atmosphere [14], and d is the distance between the object and the observer. To simplify the equation, it is a common practice to consider the extinction coefficient constant in the atmosphere [15]. Those two terms, attenuation and airlight, modify both original colors and contrast of objects present in the atmosphere [16,17]. Deweathering images is an underconstrained problem. For gray-scale images there are three unknowns for each pixel: object radiance (J), transmission of the medium (t), and airlight color component (A). For color images there are also three equations at each pixel, corresponding to the R, G, and B channels.

Several approaches have been proposed to recover images based on physical models. Most of these methods consider a single scattering process, where it is supposed that the light that reaches the observer interacts only with one localized scattering center (atmospheric particle). Single scattering is a simplification of the more realistic multiple scattering problem.

Some proposed methods presented in the literature take advantage of the fact that the airlight term is polarized at some degree [18]. These techniques take two images of the same scene with different polarization angles to approximately obtain the airlight component. Narasimhan and Nayar [19] also use two images of the scene, one of them in clear conditions to derive several geometrical constraints for assessing fog or haze color. The evident drawback of these kinds of approximations is that it is not always possible to capture two images of the same scene. To overcome this drawback, the authors use annotated image information to obtain the geometrical constraints in the scene [20]. Other authors developed methods that need the estimation of some atmospheric parameters to restore the images [10].

Recent approaches try to restore the scenes using the information contained in the image itself, avoiding the use of two images, the interaction of the user, or the knowledge of some atmospheric parameters. Some methods [12,13] have been developed based on the dark channel prior [21]. This method employs the statistics of the scene. Dark channel prior postulates that on haze-free outdoor images at least one color channel has low intensity at some pixels. He et al. [21] used this technique to obtain an approximate transmission map of the scene, evaluating the airlight and finally restoring the weather degraded image. The problem with this approximation is that the image gets tessellated. Ancuti et al. [13] improved the method comparing the hue of the original image with the hue of the inverse image to estimate the airlight color and applying a layer-base dehazing technique. Fattal [22] assessed the transmission map assuming that the albedo of the objects and the transmission are statistically uncorrelated. This method shows problems in large areas with smooth variation or in regions where the signal-to-noise ratio is low [22].

All mentioned methods are applied under not very dense fog, misty, or hazy scenes. For dense fog and objects at a certain distance to the observer (sometimes a dozen meters), there is no information to be recovered at all. In these situations, multiple scattering dominates the interactions between the atmospheric particles and all the chromatic objects' information is lost. Tao et al. [12] extend the method of dark channel prior considering the influence of multiple scattering in the atmosphere. This method needs the evaluation of the atmospheric point spread function [23] and includes convolution and deconvolution steps, which increase the computational time.

The deweathering method that we have developed in this work is based on color constancy. This property of the human visual system (HSV) accounts for the constant color appearance of objects under different illuminants changes. Different authors [24–28] have found a linear relationship with a high correlation coefficient representing, for a broad set of objects, the pairs of excitation values for each cone (L, M or S) determined for each object under two different illuminants. This linear relationship indicates that the ratio of the excitations under illuminant changes for each cone class remains roughly constant for all objects. The same ratio constancy stands for artificial sensors, as we have proved in a previous work [29].

The aim of this work is to develop a restoration algorithm for weather degraded images that is based on the response ratio constancy of the sensors of a

RGB camera. This algorithm will improve the visibility, contrast, and color in the images with no prior information about the image content and with low computational times. This paper is organized as follows. We begin by presenting our method to image deweathering problem. Our approximation is based on response ratio constancy between the channels of a camera under different illuminants. Section 3 shows the results that we have obtained with this method. We have applied our deweathering algorithm to an image database obtained under different weather conditions, ranging from mist to dense fog. This image database was obtained with a scientific and with customer cameras. We have extended the image database with artificial weather degraded images and with images collected from the Internet, where no information of capturing conditions were available. Section 4 compares our results with the other five state-of-the-art techniques. No unified quantitative method is established to evaluate or compare the quality between restored images, so we make use of five different metrics. Finally, we summarize our approach and discuss its advantages and possible limitations.

2. Method

A. Constant Ratios at Different Distances

First we have tested the linear response ratio constancy for a RGB camera when objects are viewed under two different illuminants. Next we have extended the same computations but consider that for one of the illuminants, the objects are located at a certain distance from the observer and are thus affected by the attenuation and airlight components. These computations were made using real atmospheric parameters and assuming the dichromatic atmospheric scattering model, Eq. (1).

Several authors [29,30] have shown that there is a linear relationship when the response of a sensor under a certain illuminant is depicted versus the response of the same sensor under another illuminant. These relationships occur for a variety of soft daylight spectral power distributions (SPDs) and for artificial illuminants. Romero *et al.* [29] have proved that these relationships are also preserved between the response of artificial receptors (like the ones present in RGB camera channels) under different illuminants. Depicting in the y axis the response of one camera sensor (R, G, or B digital counts of the captured image) for the illuminant present in the scene, and in the x axis the response of the same sensor under a theoretical illuminant, such as an E illuminat (i.e., an equienergetic illuminant), linear relationships appear, with a high correlation coefficient, as we have previously mentioned. Figure 1 shows an example of the response for the R channel (similar plots are obtained for G and B channels) of a calibrated scientific camera (Retiga EXi Fast 1394) for a series of samples of the Color Checker DC [31] at zero distance on an overcast day, Fig. 1(a). In the y axis is depicted the intensity of
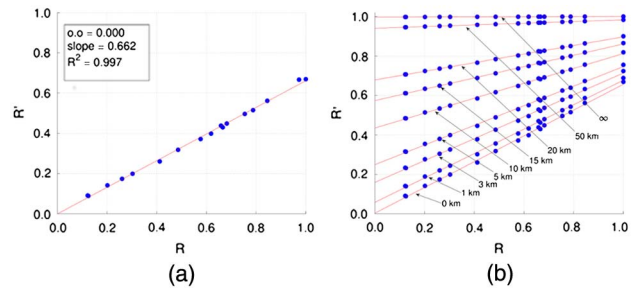

Fig. 1. (a) Relational ratio constancy response for the R channel at zero distance and (b) at several distances. As we observed in the (b) plot, as we approach to infinite distance (i.e., horizon line) excitation R' capture by the camera will remain constant for all objects.

the R channel of the captured image, and in the x axis the response of the same channel for an equienergy illuminant. The y-intercept is zero because the response of the sensor for a theoretical black object is independent of the illuminant. As the distance between the object and the observer increases, the y-intercept gets higher values as a consequence of the airlight component, Fig. 1(b). Even for a black object the airlight term causes a sensor response not equal to zero. At an infinite distance, the response of all the pixels tends to the limit value of the illuminant in the scene. Table 1 shows high correlation coefficients for 20 samples of the Color Checker DC [31] under an overcast day at several distances. Those relationships were obtained for images simulated under adverse assorted weather conditions, ranging from dense fog, mist, haze, and even dust storms. Based on the above result we propose a method based on the compensation of this added light by translating those (R, G, B) values to the ones corresponding to an ideal image, that is, to an image not affected by the atmosphere. We will assume that this ideal image would be the one illuminated with an equienergy illuminant.

B. Deweathering Algorithm

The atmospheric effects are highly dependent on the distance between the object and the observer. The proposed method has to apply the same compensation to all the pixels situated roughly at the same plane. To accomplish this previous step we have tested several approximations for image segmentation. Figure 2 shows a typical weather degraded image and the results of three clustering techniques. As a first attempt

Table 1. Data Analysis Results from Fig. 1(b)

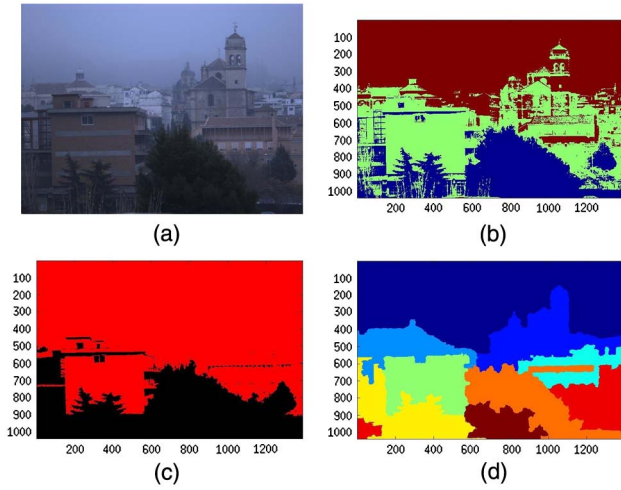| Distance (km)	y-intercept	Slope	R^2
0	0.000	0.669	0.999
1	0.057	0.663	0.999
3	0.162	0.563	0.999
5	0.256	0.501	0.999
10	0.447	0.374	1.000
15	0.589	0.279	0.999
20	0.695	0.208	0.999
50	0.949	0.036	0.991
∞	0.998	0.002	0.956

Fig. 2. Example of image segmentation with several methods: (a) original image, (b) k-means segmentation, (c) seed region growing, and (d) mean shift segmentation.

we have employed the k-means clustering technique [32]. For urban scenes, with hundred of borders and with high amount of planes this technique does not accomplish good results. Figure 2(b) shows that several objects appear mixed up in different clusters. More consistent results were obtained with the seed region growing clustering technique [33], Fig. 2(c). But these results are not good enough to be useful in such complex images. In this case only two clusters were obtained. Altering the number of seeds can increase the clusters; this alteration approximates the results obtained with k-means. Finally, we have chosen the mean shift segmentation technique [34]. This clustering technique makes a segmentation of the scene based on three parameters: one related to the maximum number of pixels allowed in the cluster, another one related to the space resolution of the clustering, and the last one related to the resolution of the color. Figure 2(d) shows the result with this technique. The objects situated approximately at different planes belong to different clusters. This clustering technique is able to obtain several clusters with an acceptable accuracy.

It is worthwhile to note that for images where the whole scene is situated approximately at a constant distance (such as aerial scenes) this previous clustering step is not necessary, so the computational time of our algorithm is reduced. For images with objects situated at far planes, once the image is segmented out in approximately equal distance planes, we can apply our intensity channel (R, G, B) correction method to different cluster regions.

The algorithm modifies the R, G, and B intensity values translating the captured RGB values (y axis) to lower ones corresponding to the intensity of a haze-free scene (x axis). In our case, this haze-free intensity value corresponds to pixel value as illuminated by an E illuminant. Those values are bounded between the minimum intensity level (0) and the maximum intensity level (255 for 8-bit images or 1 for normalized images) in the image.

Mathematically the values of the (J^c) at pixel x are defined by the following relationship for each cluster Q:

$$J^{c,Q}(x) = (I_{\text{obs}}^{c,Q}(x) - I_{\text{min}}^{c,Q})\left(\frac{I_{\text{max}}^{c,Q}}{I_{\text{max}}^{c,Q} - I_{\text{min}}^{c,Q}}\right), \quad \forall\, x \in Q, \quad (3)$$

where the superscript c stands for the channel to be processed (R, G, or B), $I_{\text{obs}}^{c,Q}$ is the intensity pixel value of the captured image, $I_{\text{min}}^{c,Q}$ is the minimum intensity value of the Qth processed cluster, and $I_{\text{max}}^{c,Q}$ is the maximum intensity value in that cluster. These maximum and minimum values would be the only two inputs of our algorithm. These two parameters have to be modeled depending on the haze intensity in the degraded image. The best parameters for each image have to be chosen by the user, based on the trial error method or in its experience. To overcome the input parameters, we employ a simple statistics to obtain them. As a first approach, a statistics based on the method box and whiskers [35] is used. With this method we are able to eliminate the outliers in the image. These outliers could be due to bad pixel response, specular reflections, or dark pixels present in the image, being not representative of the rest of scene intensity values, and modifying the final result.

Graphically the algorithm can be depicted as it is shown in Fig. 3. To simplify we have supposed just one cluster in Fig. 3, so we can omit the index Q. Our method translates the values of the pixels situated in the y axis (affected by adverse weather conditions) to the theoretical ones (not affected by adverse weather conditions) situated in the x axis, through the straight line. This straight line is defined by the two parameters of the algorithm, I_{min}^c and I_{max}^c.

This algorithm is applied channel wise, so it could be implemented as much for color as for gray-scale images. The main advantage of this method is that it could be applied without the knowledge of extra parameters.
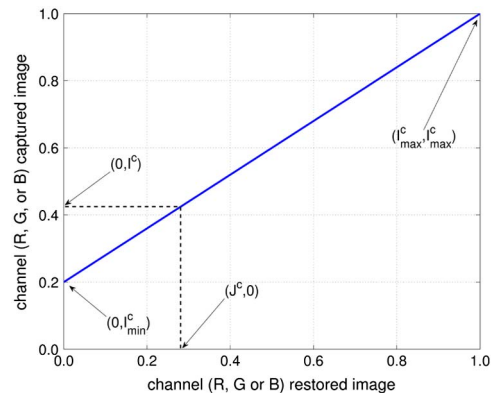

Fig. 3. Representation of the decompressing proposed model for the channels of a weather degraded image, I. The y-axis represents the intensity of the channels (R, G, or B) corresponding to the weather affected image, and the x axis represents the haze-free intensity value corresponds to pixel value as illuminated by an E illuminant. In the plot are depicted the parameters expressed by Eq. (3), supposing $Q = 1$, just one cluster.

C. Image Dataset

We test our algorithm over a set of images captured in a variety of weather conditions with a scientific calibrated camera and with customer cameras. The atmospheric conditions range from mist, haze, light fog and dense fog, to dust storms in extreme cases. These images were captured in rural scenes and in urban environments. For urban environments the scenes were composed of a wide color gamut, mainly formed by buildings situated at several distance ranges from a couple of meters to several kilometers. Rural scenes are composed of different terrain materials, forest, cultivated and noncultivated areas, and in some of them snow-capped hills.

We also extend the image set to Internet-collected images, without any kind of information provided.

3. Results

Before testing our method with real weather degraded images, we checked it over a hyperspectral database [36] with a simulated fog, Fig. 4(a). These simulations were carried out using the dichromatic atmospheric scattering model with real extinction coefficients at several distances. For these images our method get very good results as can be observed in Fig. 4(b). In this case there is no need for image segmentation as the objects are considered to be located at the same plane. We did not take into account any kind of point-wise degradation or noise estimation in the simulations, as we only tested the color restoration performance of our method.

Figure 5(a) shows an image captured with a commercial RGB camera on a misty day. The scene corresponds to a rural image with some artificial objects in it. Prior to image restoration, we used the mean shift segmentation algorithm [34] to approximately find out the different distant planes contained in the scene, Fig. 5(b). As it is shown in Fig. 5(c), when the clustering algorithm is employed some artifacts appear in the recovered image. These artifacts correspond to discontinuities between different clusters.

Figure 6 corresponds to a hazy day with objects situated at several planes. This image was captured with a scientific camera. The recovered image was obtained using the aforementioned box and whiskers statistical method. In the restored image the background becomes distinguishable, showing some
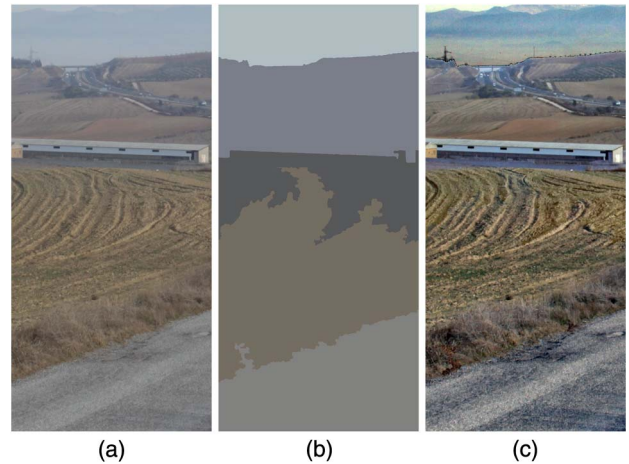

Fig. 5. (a) Rural scene captured on a misty day, (b) result of the mean shift segmentation application, and (c) recovered image with the proposed method.

Fig. 6. (a) Urban scene captured on a foggy day and (b) restored image applying the proposed method in automatic mode.

buildings and a forest, while the objects in near planes appear more contrasted.

Figure 7 shows some examples of the results for this algorithm under very dense fog conditions. This is a quite extreme case where the objects in the original image are hardly visible. For images captured under these conditions this method is able to restore only some portions of them as the density of the fog

Fig. 4. (a) Dichromatic atmospheric fog simulated image at a distance of 10 km and (b) recovered image with the proposed method.
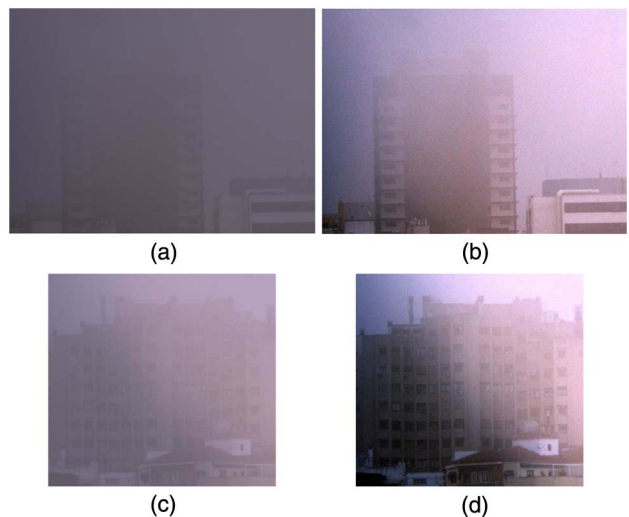

Fig. 7. (a), (c) Urban scenes captured under severe fog. (b), (d) Restored images applying the proposed method.

could change across the same plane. The method is able to recover some colors of the buildings that are completely lost in the foggy images. In such a dense fog images we can suppose that the objects are situated not so far from the observer (no information reaches the observer from distant objects). Under this assumption, the clustering algorithm is useless and we can apply our method directly.

We also apply our restoration algorithm to images captured under dust storms. These conditions correspond to more tricky situations. The particle sizes are bigger than in fog conditions and the shape of these dust particles are more heterogeneous. For that reason, the interactions between the light and the particles are physically more complex than in fog conditions.

Figures 8(a) and 8(c) were captured with a customer reflex camera under a dust storm in the city of Granada, Spain. These images are composed of a huge amount of objects, enormous number of borders, and a wide color gamut. Despite the complexity of the images, our approximation is able to increase the contrast of the objects maintaining good color fidelity. We were able to restore Fig. 8(b) without the aim of a clustering method, even with the high distance between foreground and background objects in the scene.

When the objects on the scene are situated far away from the observer, it can be also considered that

Fig. 9. (a) Far away scene captured with a commercial camera and (b) automatic restored image with the proposed method.

they are at the same plane. Under these situations it is not necessary to segment out the image and we can apply our algorithm directly. Figure 9 corresponds to a rural scene captured under a hazy day with a customer camera. The terrain structure of the mountains becomes distinguishable, as does a path situated in the foreground centred hill not visible in the original image.

Aerial images accomplish with the low depth condition. Figure 10 shows an example of this kind of restoration. This image was obtained from the Internet without extra information of atmospheric conditions [37]. The restored counterpart was obtained applying our method without any segmentation algorithm. In the restored image forest zones are clearly identified over the cultivated areas.

All the operations in this restoration technique over the pixels in the image are linear, obtaining computational times below 1 s for images of 1038 × 1390 pixels. This algorithm was implemented in MATLAB 64-bit on a personal computer equipped with Intel Core 2 Quad Q9550 processor and 4 GB of RAM memory.

4. Discussion and Conclusions

We have presented a dehazing method based on camera sensor response ratio constancy. This method obtains good results over atmospheric degraded images in a wide range of adverse conditions. We have tested our method on images captured with a calibrated scientific camera, customer cameras, and even with Internet images. The results vary depending on the
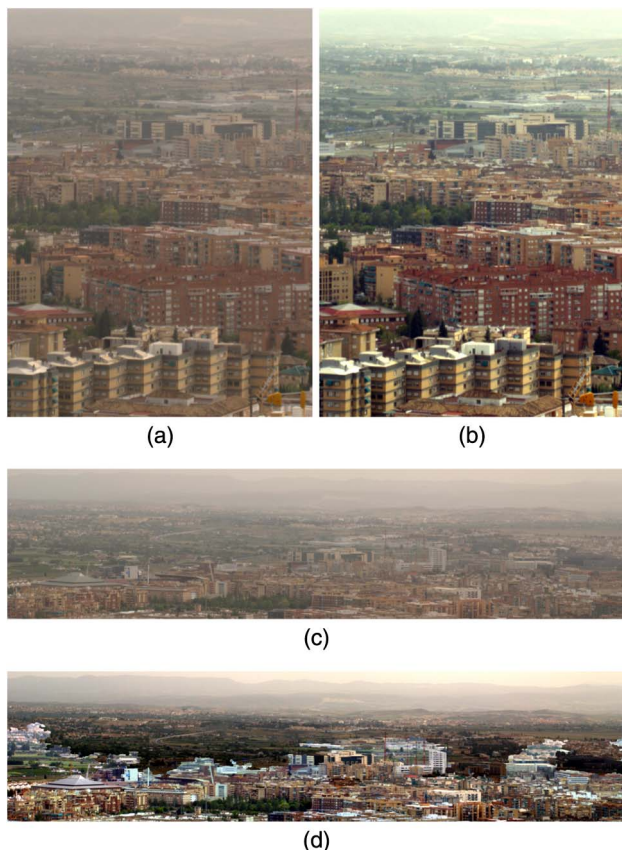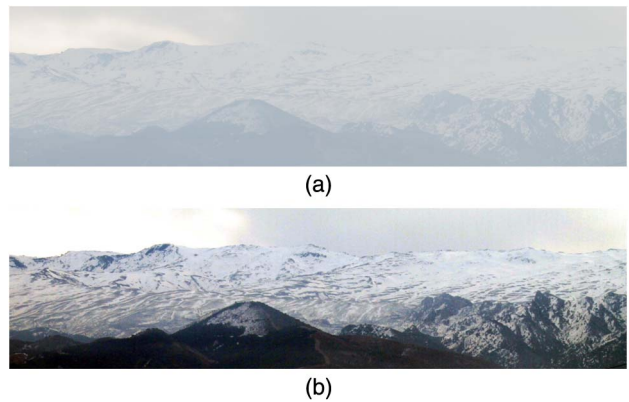

Fig. 8. (a), (c) Images captured under a dust storm in Granada (Spain). (b) Restored image employing our method without the segmentation step, and (d) restored image employing our algorithm with a previous segmentation step.

Fig. 10. (a) Aerial foggy image and (b) automatic restored image with the proposed method.

adverse conditions present in the scenes. For light fog, mist and hazy conditions, our result gets good color restoration.

This technique can be applied to both color and gray-scale images. But there is no standard metric to evaluate and/or compare the quality between restored images. Since weather effects are volumetric, classical image noise or degradation evaluation techniques, where the effect is added and then removed, are not suitable for evaluating weather degraded images [38]. Thus we make use of five different metrics present in the literature to test the performance of our algorithm and to compare it with the methods proposed by other authors. These metrics do not use any kind of subjective evaluation and can be described as follows:

• Laplacian (Lap) and Gray Mean Gradient (GMG) [39,40] will be used to compute the textures of the images, especially the edge information of the image. Higher values of both metrics will suggest finest textures in the image.

• Descriptor **e** [38] measures the number of visible edges in the restored image regarding the original one. Higher values means more visible edges in the restored image.

• Descriptor $\bar{r}$ [38] computes the geometric mean of the ratios of the visible edges, that is, expresses the quality of the contrast restoration by the proposed method. Higher values mean better contrast restoration.

• Descriptor σ [38] computes the number of pixels that are saturated (i.e., black or white) after applying the deweathering algorithm but were not before. This metric is quite useful since the recovering algorithms are prone to saturate pixels (pixels get completely black for dark objects and completely white for light objects).

The Lap, GMG, **e**, and $\bar{r}$ metrics evaluate the improvement over the visible edges or textures in the restored image. As opposed to the aforementioned metrics, higher values in Descriptor σ means worst restored image.

We have to point out that the purpose of our method is not to obtain a pleasant image for the observer, but to achieve an image with a low haze component and more contrasted objects. If we were able to completely remove the effect of the atmosphere over an image, the depth sensation could disappear, resulting in an artificial restored image. He *et al.* [21] keeps some haze component to maintain the aerial perspective and get a more realistic image. We have compared our approach with six other authors' work [12,13,15,21, 22,41]. Thus we have used the images available from the web pages of the authors or the ones available in published papers to test our approximation to the weather recovering issue. The quality of these images are not so good as most of the authors employ low-resolution images (usually between 600 × 480 to 800 × 600 pixels) to test their algorithms.

Table 2.   Image Quality Assessment Result for Images in Fig. 11 (the Number in Bold Denotes the Best Value of Each Row)

Metric	Input Image	Ancuti's Result	He's Result	Our Result
Lap	19.59	**58.91**	39.70	48.52
GMG	4.30	**11.98**	8.30	10.41
Descriptor **e**	—	**1.60**	1.35	1.11
Descriptor σ	—	2.23%	**0.03%**	0.23%
Descriptor $\bar{r}$	—	**2.97**	1.97	2.61

Table 3.   Image Quality Assessment Result for Images in Fig. 12 (the Number in Bold Denotes the Best Value of Each Row)

Metric	Input Image	Tarel's Result	He's Result	Fattal's Result	Tan's Result	Our Result
Lap	58.02	99.55	80.95	72.12	**135.47**	103.72
GMG	10.89	18.50	15.05	13.46	**24.34**	19.17
Descriptor **e**	—	**0.07**	0.04	0.05	**0.07**	0.01
Descriptor σ	—	**0.00%**	**0.00%**	0.37%	1.16%	0.04%
Descriptor $\bar{r}$	—	1.81	1.40	1.29	**2.18**	1.77

Tables 2–5 summarize the results of the application of the aforementioned metrics for different images and algorithms.

Table 2 shows that our method is close to the Ancuti's [13] algorithm for the recovering of Fig. 11. The Ancuti's method gets the best performance for Lap, GMG, **e**, and $\bar{r}$ metrics, i.e., those metrics related to the restored edges. Nevertheless, this method obtains clearly more saturated pixels ($\sigma = 2.23\%$) than our technique ($\sigma = 0.23\%$), as it can be observed in the railways of the figure. On the other hand, He [21] obtains the best result for Descriptor σ.

Figure 12 shows the result of five different recovering methods for an urban scene on a hazy day. In this case our method restores the image without introducing distorting effects around the horizon region; we achieve good performance in the rest of the areas of the scene. Table 3 show that Tan's method gets the higher figures for the Lap, GMG,
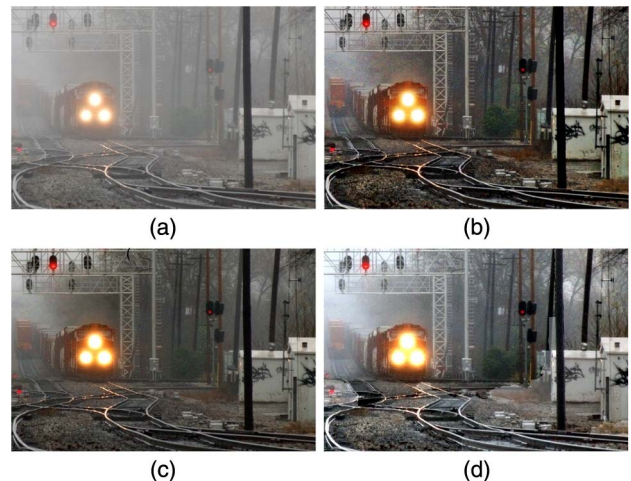

Fig. 11.   (a) Original image, (b) results by Ancuti [13], (c) He [21], and (d) proposed method.
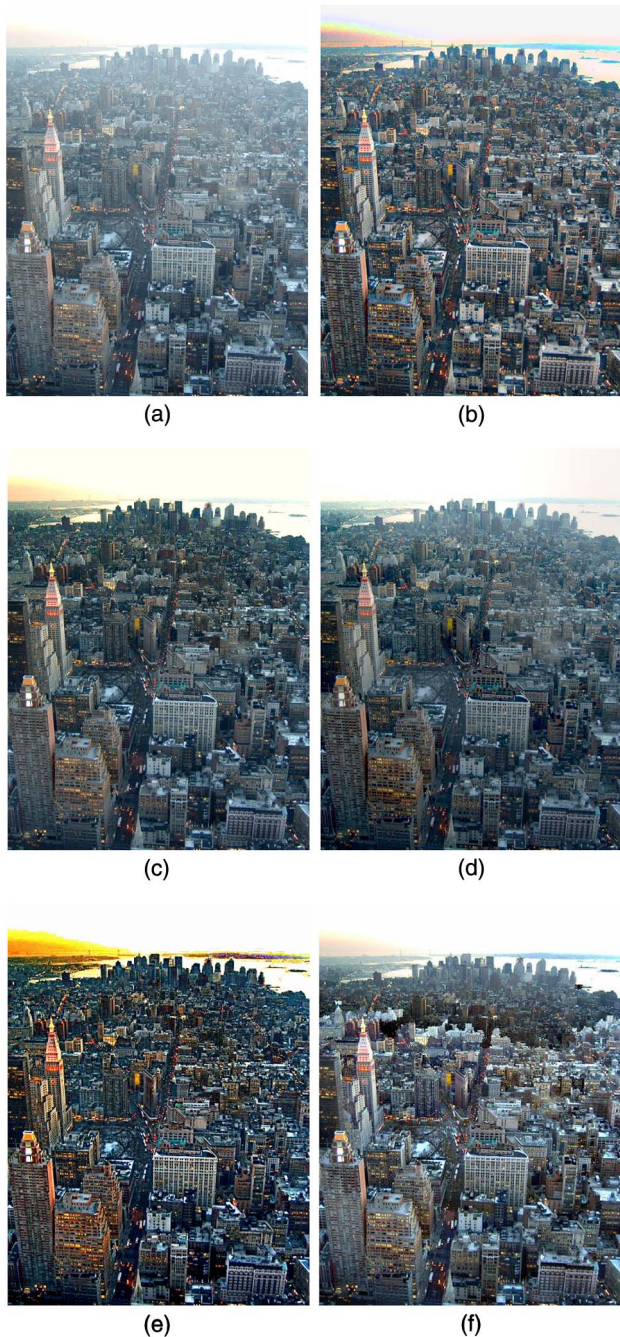
Fig. 12. (a) Original image, (b) results by Tarel [41], (c) He [21], (d) Fattal [22], (e) Tan [15], (f) proposed method.

and r̄ metrics, but obtains the worst result for Descriptor σ.

Figure 13 shows that our method is able also to restore misty scenes as the other methods do. The apparently good result from Fattal's method, with high values for Lap, GMG, and r̄ metrics, show on the contrary that this algorithm will produce dark pixels in some regions of the images ($\sigma = 9.34\%$ clearly over the 0% obtained using both the He and our algorithm). The pixels corresponding to the summit of the mountains get dimmed in Fattal's restored image, where the other two obtain good results.
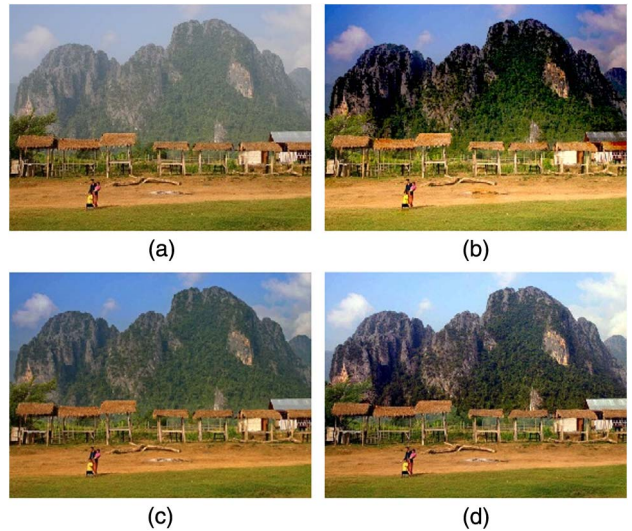

Fig. 13. (a) Original image, (b) results by Fattal [22], (c) He [21], and (d) proposed method.

Finally, we have compared our result with one of the latest proposed techniques. Table 4 includes new results from Tao's model [12]. Our method obtains higher figures for Lap, GMG, and clearly improve Descriptor **e** (**e** = 60.29 and **e** = 35.40 for our method and Tao's proposal, respectively). Over aerial images, our method obtains good color and contrast restoration, as Fig. 14 shows.

A general behavior showing up in the aforementioned results is that in most of the cases, higher figures for the Lap, GMG, **e**, and r̄ metrics involve more saturated pixels in the restored images. Nonetheless our method obtains good results, keeping low values for the saturated pixels. Anyway, all of these techniques improve the original degraded images on some level. In spite of the fact that the proposed technique does not always obtain the best performance, the restored images are close to the best technique for all tested images, and for some images and metrics the best results. The main advantages of the proposed method rely on its simplicity and good color recovery performance.

In general, the technique proposed in this work gets better results for near objects than the other authors' work, obtaining more contrasted object and with more realistic colors over tested images. On the contrary, at high distances the results depend on the kind of images and the weather conditions.

A human observer could find a mismatch between the figures obtained in Tables 2–5 and the quality of

Table 4. Image Quality Assessment Result for Images in Fig. 14 (the Number in Bold Denotes the Best Value of Each Row)

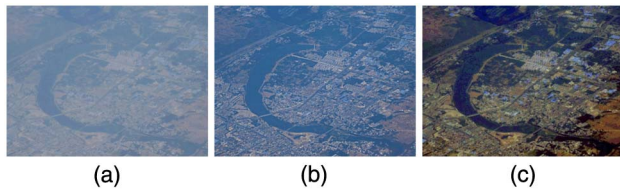| Metric	Input Image	Tao's Result	Our Result
Lap	6.95	15.24	**17.36**
GMG	1.61	4.33	**5.02**
Descriptor **e**	—	35.40	**60.29**
Descriptor σ	—	**0.00%**	**0.00%**
Descriptor r̄	—	**4.42**	3.62

Fig. 14. (a) Original image, (b) results by Tao [12], and (c) proposed method.

Table 5. Image Quality Assessment Result for Images in Fig. 13 (the Number in Bold Denotes the Best Value of Each Row)

Metric	Input Image	Fattal's Result	He's Result	Our Result
Lap	47.45	**80.48**	53.50	72.91
GMG	8.65	**14.34**	9.81	13.24
Descriptor e	—	0.10	**0.15**	0.05
Descriptor σ	—	9.34%	**0.00%**	0.03%
Descriptor $\bar{r}$	—	**1.72**	1.18	1.64

the images. The employed metrics evaluate the improvement of the images from an objective point of view, not considering any kind of subjective evaluation. As we previously mentioned, up to now no subjective metric is available to evaluate the performance of weather recovering algorithms. A new metric capable of evaluating not only the edges, the texture, and the saturated pixels on the restored image, but what a human observer could judge as a pleasant image needs to be further studied and developed.

References

1. M. Minnaert, *The Nature of Light and Colour in the Open Air* (Dover, 1954).
2. S. D. Gedzelman, "Atmospheric optics in art," Appl. Opt. **30**, 3514–3522 (1991).
3. C. F. Bohren, *Atmospheric Optics* (Wiley, 2004).
4. R. L. Lee, Jr., "Measuring overcast colors with all-sky imaging," Appl. Opt. **47**, H106–H115 (2008).
5. S. G. Narasimhan and S. K. Nayar, "Interactive (de) weathering of an image using physical models," in *IEEE Workshop on Color and Photometric Methods in Computer Vision* (IEEE, 2003), Vol. **6**, p. 1.
6. J. A. Stark, "Adaptive image contrast enhancement using generalizations of histogram equalization," IEEE Trans. Image Process. **9**, 889–896 (2000).
7. H. Zhu, F. H. Chan, and F. K. Lam, "Image contrast enhancement by constrained local histogram equalization," Comput. Vision Image Understanding **73**, 281–290 (1999).
8. K. Joshi and R. Kamathe, "Quantification of retinex in enhancement of weather degraded images," in *IEEE International Conference on Audio, Language and Image Processing* (IEEE, 2008), pp. 1229–1233.
9. G. Hines, Z. Rahman, D. Jobson, and G. Woodell, "Single-scale retinex using digital signal processors," in *Global Signal Processing Conference* (2004), Vol. **27**, pp. 1–6.
10. K. Tan and J. P. Oakley, "Physics-based approach to color image enhancement in poor visibility conditions," J. Opt. Soc. Am. A **18**, 2460–2467 (2001).
11. S. G. Narasimhan and S. K. Nayar, "Chromatic framework for vision in bad weather," in *Proceedings of IEEE Conference on Computer Vision and Pattern Recognition, 2000* (IEEE, 2000), Vol. **1**, pp. 598–605.
12. S. Tao, H. Feng, Z. Xu, and Q. Li, "Image degradation and recovery based on multiple scattering in remote sensing and bad weather condition," Opt. Express **20**, 16584–16595 (2012).
13. C. O. Ancuti, C. Ancuti, C. Hermans, and P. Bekaert, "A fast semi-inverse approach to detect and remove the haze from a single image," in *Computer Vision–ACCV 2010* (Springer, 2011), pp. 501–514.
14. J. Lenoble, *Atmospheric Radiative Transfer, Studies in Geophysical Optics and Remote Sensing* (A. Deepak, 1993).
15. R. T. Tan, "Visibility in bad weather from a single image," in *IEEE Conference on Computer Vision and Pattern Recognition* (IEEE, 2008), pp. 1–8.
16. J. Romero, R. Luzón-González, J. L. Nieves, and J. Hernández-Andrés, "Color changes in objects in natural scenes as a function of observation distance and weather conditions," Appl. Opt. **50**, F112–F120 (2011).
17. R. Luzón-González, S. Nascimento, O. Masuda, and J. Romero, "Chromatic losses in natural scenes with viewing distance," Color Res. Appl. **39**, 341–346 (2014).
18. T. Treibitz and Y. Y. Schechner, "Polarization: beneficial for visibility enhancement?" in *IEEE Conference on Computer Vision and Pattern Recognition* (IEEE, 2009), pp. 525–532.
19. S. K. Nayar and S. G. Narasimhan, "Vision in bad weather," in *Proceedings of the Seventh IEEE International Conference on Computer Vision* (IEEE, 1999), Vol. **2**, pp. 820–827.
20. S. G. Narasimhan and S. K. Nayar, "Contrast restoration of weather degraded images," IEEE Trans. Pattern Anal. Mach. Intell. **25**, 713–724 (2003).
21. K. He, J. Sun, and X. Tang, "Single image haze removal using dark channel prior," IEEE Trans. Pattern Anal. Mach. Intell. **33**, 2341–2353 (2011).
22. R. Fattal, "Single image dehazing," in *Proceedings of ACM Transactions on Graphics (TOG)* (ACM, 2008), Vol. **27**, p. 72.
23. S. G. Narasimhan and S. K. Nayar, "Shedding light on the weather," in *IEEE Computer Society Conference on Computer Vision and Pattern Recognition* (IEEE, 2003), Vol. **1**, pp. 665–672.
24. J. L. Dannemiller, "Rank orderings of photoreceptor photon catches from natural objects are nearly illuminant-invariant," Vis. Res. **33**, 131–140 (1993).
25. D. H. Foster and S. M. Nascimento, "Relational colour constancy from invariant cone-excitation ratios," Proc. R. Soc. B **257**, 115–121 (1994).
26. Q. Zaidi, B. Spehar, and J. DeBonet, "Color constancy in variegated scenes: role of low-level mechanisms in discounting illumination changes," J. Opt. Soc. Am. A **14**, 2608–2621 (1997).
27. Q. Zaidi, "Identification of illuminant and object colors: heuristic-based algorithms," J. Opt. Soc. Am. A **15**, 1767–1776 (1998).
28. S. Nascimento, F. P. Ferreira, and D. H. Foster, "Statistics of spatial cone-excitation ratios in natural scenes," J. Opt. Soc. Am. A **19**, 1484–1490 (2002).
29. J. Romero, D. Partal, J. L. Nieves, and J. Hernández-Andrés, "Sensor-response-ratio constancy under changes in natural and artificial illuminants," Color Res. Appl. **32**, 284–292 (2007).
30. C. F. Borges, "Trichromatic approximation method for surface illumination," J. Opt. Soc. Am. A **8**, 1319–1323 (1991).
31. GretagMacbeth ColorChecker DC Chart (GretagMacBeth, 2004).
32. S. Ray and R. H. Turi, "Determination of number of clusters in k-means clustering and application in colour image segmentation," in *Proceedings of the 4th International Conference on Advances in Pattern Recognition and Digital Techniques* (1999), pp. 137–143.
33. R. Adams and L. Bischof, "Seeded region growing," IEEE Trans. Pattern Anal. Mach. Intell. **16**, 641–647 (1994).

34. D. Comaniciu and P. Meer, "Mean shift: a robust approach toward feature space analysis," IEEE Trans. Pattern Anal. Mach. Intell. **24**, 603–619 (2002).

35. J. M. Chambers, *Graphical Methods for Data Analysis* (Chapman & Hall/CRC Press, 1983).

36. J. M. M. Linhares, P. D. Pinto, and S. M. C. Nascimento, "The number of discernible colors in natural scenes," J. Opt. Soc. Am. A **25**, 2918–2924 (2008).

37. https://commons.wikimedia.org/wiki/File:Aerial-photo-heavy-haze.jpg (01 July 2014).

38. N. Hautière, J.-P. Tarel, D. Aubert, and E. Dumont, "Blind contrast enhancement assessment by gradient ratioing at visible edges," Image Anal. Stereol. J. **27**, 87–95 (2008).

39. Y. Chen, Z. Xu, H. Feng, and Q. Li, "Image stabilization with support vector machine," J. Zhejiang Univ. Sci. C **12**, 478–485 (2011).

40. Y.-Q. Zhang, Y. Ding, J.-S. Xiao, J. Liu, and Z. Guo, "Visibility enhancement using an image filtering approach," EURASIP J. Adv. Signal Process. **2012**, 1–6 (2012).

41. J.-P. Tarel and N. Hautière, "Fast visibility restoration from a single color or gray level image," in *IEEE 12th International Conference on Computer Vision* (IEEE, 2009), pp. 2201–2208.